doi.org/10.26398/IJAS.0032-014

AN APPLICATION OF SPATIALLY ADJUSTED KOLMOGOROV-SMIRNOV TEST IN COMPARING HEART PET SCANS

Wenjun Zheng, Dejian Lai[1]

Department of Biostatistics and Data Science, School of Public Health, The University of Texas Health Science Center at Houston, 1200 Pressler Street, Houston, Texas, USA

Zhe Wang

Human Genetics Center, The University of Texas Health Science Center at Houston, 1200 Pressler Street, Houston, Texas, USA

Nils P. Johnson, K. Lance Gould

Weatherhead PET Imaging Center, McGovern Medical School, The University of Texas Health Science Center at Houston, 6431 Fannin Street, Houston, Texas, USA

Abstract *The Kolmogorov-Smirnov (KS) test has been popular in many applied fields. Published research has suggested the utility of the KS test in image processing, histogram analysis, and PET/CT scans. However, the fundamental assumption of independence in a statistical model is easily overlooked. When the KS test is applied to spatial analysis, autocorrelation may cause the KS test to have an inflated type I error (small p-values) if no adjustments for spatial correlation are applied. To adjust for autocorrelation, the KS test must incorporate spatial adjustment. The spatially-adjusted KS has a controlled type I error and non-inferior power compared to the original KS test. Utilizing the KS test with spatial adjustment, we reanalyzed a trial comparing two types of stress medications: regadenoson (administered using different timings) versus dipyridamole. To analyze the PET scans with spatial autocorrelation, we introduced a novel way of reconstructing the shape of the human heart using spherical coordinates, and compared the KS test with spatial adjustment to a KS test with adjustment for correlation. The results showed that the reconstructed PET scans analyzed by the KS test with spatial adjustment have controlled p-values.*

Keywords: *Kolmogorov-Smirnov, Cardiovascular disease, PET, Spatial autocorrelation.*

[1] Corresponding author, e-mail: Dejian.Lai@uth.tmc.edu

1. INTRODUCTION

In order to integrate coronary flow reserve (CFR) with absolute stress blood flow, a new concept termed coronary flow capacity (CFC) was developed at the Weatherhead PET Imaging Center of the University of Texas Health Science Center at Houston and approved by the Food and Drug Administration (FDA) based on a comprehensive scientific review. Several published reports validated the concept and proved its effects as a biomarker for cardiovascular disease prognosis (Gould and Johnson, 2018).

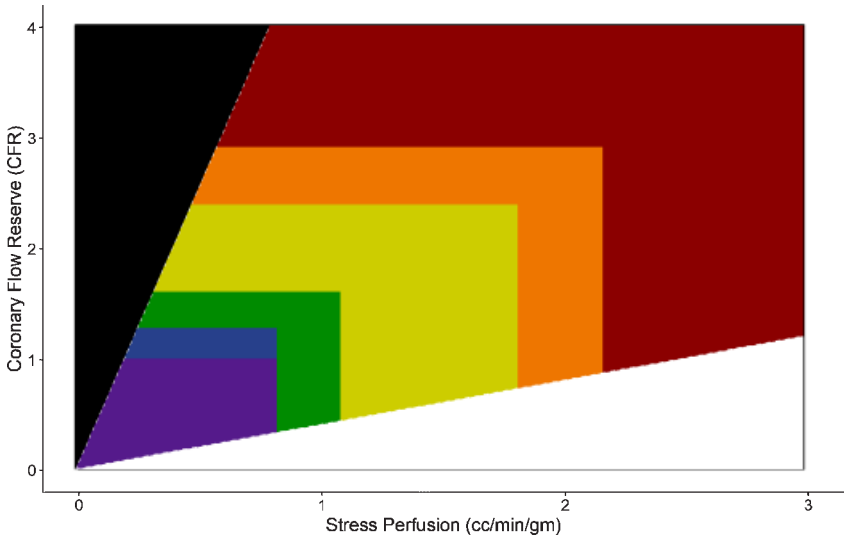

Fig. 1: CFC Scatter Plot of CFR versus Absolute Stress Flow

As shown in Figure 1, we know that when CFR (the unitless ratio of stress to rest perfusion) is larger than 2.9 or stress perfusion is more than 2.17 (units of volume per time per amount of tissue, here cc/min/g) then the CFC is coded as excellent and the color code is red; CFR from 2.38 to 2.9 or perfusion from 1.82 to 2.17 represents typical CFC colored orange; CFR from 1.6 to 2.38 or stress perfusion from 1.09 to 1.82 indicates mildly reduced CFC colored yellow; CFR 1.27 to 1.6 or stress perfusion from 0.83 to 1.09 describes moderately reduced CFC colored green; CFR from 1 to 1.27 or stress perfusion less than 0.83 marks severely reduced CFC colored blue; and lastly when CFR is less than 1, then myocardial steal exists and is colored purple. The black triangle in the upper left and white triangle at the bottom represent the lower limit of rest flow for

viability and the upper limit of clinically observed rest flow, respectively (Gould and Johnson, 2018).

The KS test has been popular in many fields of application. It is a non-parametric method under simple settings, with no assumptions about the distribution of tested data. It measures the supremum of the absolute divergence of empirical distribution functions (EDF) between the dataset of interest and the second dataset (Smirnov, 1939). The test has been widely applied for testing the equality of distributions. In addition, the EDF test tends to give higher power than the χ^2 test (Pettitt and Stephens, 1977).

Given variable $X : x_1, x_2, \ldots, x_{n-1}, x_n$ and $Y : y_1, y_2, \ldots, y_{m-1}, y_m$ with sample size of n and m, respectively, the original one-sample and two-sample KS statistic has the form as follows (Kolmogorov, 1933; Smirnov, 1939).

$$K_n = \sqrt{n} \sup_x |F_n(x) - F(x)|, \tag{1}$$

$$K_{m,n} = \sqrt{\frac{mn}{m+n}} \sup_x |F_n(x) - G_m(x)| \tag{2}$$

where, $F(x)$ is the cumulative density function. $F_n(x)$ and $G_m(x)$ are the EDFs for variable X and Y, respectively. That is, $F(x) = P(X \leq x)$, $F_n(x) = \frac{1}{n} \sum_{i=1}^{n} I(x_i \leq x)$ and $G_m(x) = \frac{1}{m} \sum_{j=1}^{m} I(y_j \leq x)$ and $I(x_i \leq x)$ is the indicator function.

The KS test has been used to discriminate image differences. Published papers have applied the KS test to image processing and histogram analysis (Lampariello, 2000). Lim showed that the KS test has a relatively higher power compared to Wilcoxon and t-tests when the variation is relatively large (Lim and Jang, 2002). Geman used the KS test for discriminating homogeneous maps by pixel gray level distribution (Geman et al., 1990). In clinical fields, published reports suggest that the KS test was valid for comparing magnetic resonance (MR) images (Baselice, 2017; Chen et al., 2006; Rajan et al., 2014). Kipritidis used the KS test for CT/PET scans and Brook applied histogram analysis with KS for spectral CT scans to evaluate artifact reduction (Brook et al., 2012; Kipritidis et al., 2016). However, the fundamental assumption of independence in a statistical model is easily overlooked. Without adjusting for correlations between samples, positive linear correlations may result in a conservative estimate of type I error using the KS test and negative linear correlations may cause a liberal type I error (> 0.05) (Weiss, 1978; Zheng et al., 2019). When the KS test is applied to spatial analysis with the assumption of independence, autocorrelation may cause the KS test to have a larger type I error with smaller p-values if no adjustments are made for spatial autocorrelation.

Under positive spatial autocorrelation, the locations closer to each other tend to be similar and dependent; locations further away tend to be more independent. Therefore, the effective sample size under spatial autocorrelation may be different than the original sample size (Cressie, 1992). We label the true sample size under spatial autocorrelation as an informative sample size $n^{'}$. To adjust for spatial autocorrelation, we derive the KS test with spatial adjustment (Zheng and Lai, 2019). The KS test with spatial adjustment has an informative sample size $n^{'}$.

$$n^{'} = n \times \frac{2}{1 + e^{3.934I + 3.172I^3}} \tag{3}$$

Here, I is the Moran's I that measures the spatial autocorrelation of N spatial subjects defined as $I = \frac{N}{S} \frac{\sum_{i=1}^{N} \sum_{j=1}^{N} w_{ij}(x_i - \mu)(x_j - \mu)}{\sum_{j=1}^{N} (x_i - \mu)^2}$, where w_{ij} denotes the preset weight between i^{th} and j^{th} subjects (Moran, 1950), $S = \sum_{i=1}^{N} \sum_{j=1}^{N} w_{ij}$ and $\mu = \bar{X} = \sum_{i=1}^{N} x_i / N$. One of the common weight functions w_{ij} is the squared inverse distance $w_{ij} = \frac{1}{(dist(s_i, s_j))^2}$ (Shepard, 1968).

Given the informative sample size, the one-sample KS statistic $K^*_{n'}$ with spatial adjustment for autocorrelation and the two-sample KS statistic $K^*_{m',n'}$ with spatial adjustment for autocorrelation are defined as follows.

$$K^*_{n'} = \sqrt{n'} \sup_x |F_n(x) - F(x)| \tag{4}$$

$$K^*_{m',n'} = \sqrt{\frac{m'n'}{m' + n'}} \sup_x |F_n(x) - G_m(x)| \tag{5}$$

The other popular test for analyzing a positron emission tomography (PET) scan is the t-test (Kershah et al., 2013). The t-test takes the sample mean and error of the mean to compare the dataset of interest and determine if there are significant differences (Student, 1908). The general t-test may be written as $t = (\bar{X} - \mu)/(\frac{s}{\sqrt{n}})$, where $s = \frac{1}{n-1} \sum_{i=1}^{n} (x_i - \bar{X})^2$. Here, $\bar{X}$ is the sample mean of $X: x_1, x_2, \ldots, x_n$; s is the estimated standard deviation and μ is the population mean. A commonly used type of t-test for comparing scans in cardiac imaging is the paired t-test (Aston et al., 2000; DeKemp et al., 2000).

$$t = (\bar{X}_d - 0)/(\frac{s_d}{\sqrt{n}}) \tag{6}$$

The sample mean $\bar{X}_d$ of the difference for the paired samples $X_d: (x_{1,1} - x_{2,1}), (x_{1,2} - x_{2,2}), \ldots, (x_{1,n} - x_{2,n})$, s_d is the standard error of mean.

To compare cardiac PET scans, we applied the KS test with spatial adjustment via Moran's I on the averaged pixel distribution of CFC and compared the results to the t-test in its original form.

2. METHODS

The geometry of the heart plays a critical role in the mechanics of cardiology. In 1892, Woods used a spherical coordinate system to mimic the heart shape (Woods, 1892). Since then, the sphericity index system has been used by several studies to reconstruct the shape of heart (Mitchell et al., 1992). Azhari used a special normalized helical shape descriptor, term a "geometrical cardiogra", to determine the shape of left ventricle (Azhari et al., 1999). A spherical shape has proven to approximate the shape of the heart (Hansen et al., 2002). It has also been suggested that the shape of the left ventricle resembles a truncated ellipsoid (Adhyapak and Parachuri, 2010; Udelson, 2017). Several strategies have successfully modeled the left ventricle using a truncated ellipsoid (Adhyapak et al., 2013; Bozkurt, 2019).

In our study, we reconstructed cardiac geometry from PET imaging data using a Cartesian coordinate system. PET-CT is a powerful tool that combines PET (positron emission tomography) and computed tomography (CT) scans. It images left ventricular CFR and stress perfusion along 21 long-axis slices each with 64 radial sections around the short axis.

To represent the cardiac shape from the PET data, we simulated a three dimensional space with fixed locations D generated to represent the location imaged flow parameters. The three-dimensional space is commonly represented by the symbol $\boldsymbol{R^3}$ (Herman and Strang, 2016). Spherical coordinates were used to visually present the simulated $\boldsymbol{R^3}$ space (see Figure 2).

A gridded map in the shape of a truncated ellipsoid, similar to a half football, was used to match the fixed locations $D = (X, Y, Z)$. We generated realizations of fixed locations D in $\boldsymbol{R^3}$ given the spherical coordinates system (ρ, θ, ϕ) using the followed algorithms.

1. A truncated ellipsoid with radius of one unit, $\rho = 1$, was simulated. Vertical coordinates Φ of the simulated points in the spherical coordinates system were generated by dividing the vertical plane. In the vertical plane, equally divide the area of $(\pi/2, \pi)$ into 21 pieces to resemble the slices along the long axis of the left ventricle as imaged by cardiac PET.

$$\Phi = (\phi_1, \phi_2, \ldots, \phi_{21}) = (\frac{21}{42}\pi, \frac{22}{42}\pi, \ldots, \frac{41}{42}\pi).$$

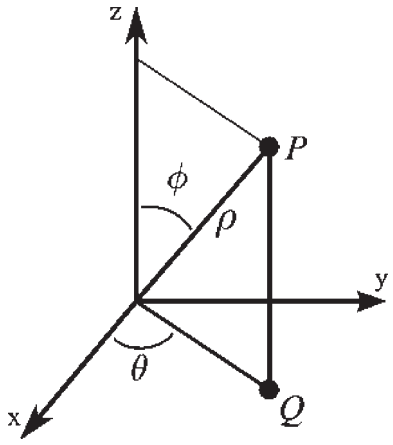

Fig. 2: Spherical Coordinates

2. Similarly, horizontal coordinates Θ were calculated by equally dividing a circle into 64 pieces to resemble the segments of the of each short axis slices as imaged by cardiac PET.

$$\Theta = (\theta_1, \theta_2, \ldots, \theta_{64}) = (\frac{1}{32}\pi, \frac{2}{32}\pi, \ldots, 2\pi).$$

3. Transform spherical coordinates into Cartesian coordinates using the following formulae.

$$\begin{aligned} x &= \rho \sin\phi \cos\theta \\ y &= \rho \sin\phi \sin\theta \\ z &= \rho \cos\phi \end{aligned}$$

The truncated ellipsoid in 3-D space was generated in Figure 3 using the above algorithm. The distance between each unique pair of locations was calculated using these coordinates. We defined the arc length between two locations as the distance of interest.

The distance between two locations $s_i = (x_i, y_i, z_i) = (\rho \sin\phi_i \cos\theta_i, \rho \sin\phi_i \sin\theta_i, \rho \cos\phi_i)$ and $s_j = (x_j, y_j, z_j) = (\rho \sin\phi_j \cos\theta_j, \rho \sin\phi_j \sin\theta_j, \rho \cos\phi_j)$ can be written as below.

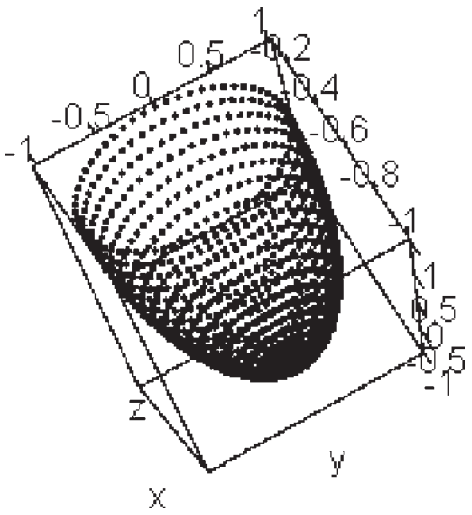

Fig. 3: Generated coordinates for reconstructing PET using a truncated ellipsoid shape

$$Acos = \arccos(\cos\phi_i \cos\phi_j + \sin\phi_i \sin\phi_j \cos(\theta_i - \theta_j)) \tag{7}$$

$$dist(s_i, s_j) = \begin{cases} \rho \times \arccos(1), & \text{Acos} \geq 1 \\ \rho \times \arccos(-1), & \text{Acos} \leq 1 \\ \rho \times Acos, & \text{otherwise} \end{cases} \tag{8}$$

PET data was placed into the model shown in figure 3 with respect to the column and row order. The spatial autocorrelation coefficient, Moran's I, was computed for the reconstructed PET data. Using the reconstructed model, the KS analysis with adjustment for spatial autocorrelation was carried and the informative sample size was calculated with equation (3).

2.1. DATA COLLECTION

Recruited subjects were split into 6 groups, and each group went through a two-stage PET imaging procedure. The first group of subjects was administered dipyridamole in both stages of PET scans. The other groups of subjects were administered regadenoson for one scan and dipyridamole for the other, with varying time delays between regadenoson administration and the injection of the PET radio-

tracer. The protocol for the trial is described in Figure 4 and Table 1. In this single-subject design, subjects imaged using dipyridamole stress were compared with themselves using either repeated dipyridamole or regadenoson but variable timing delays.

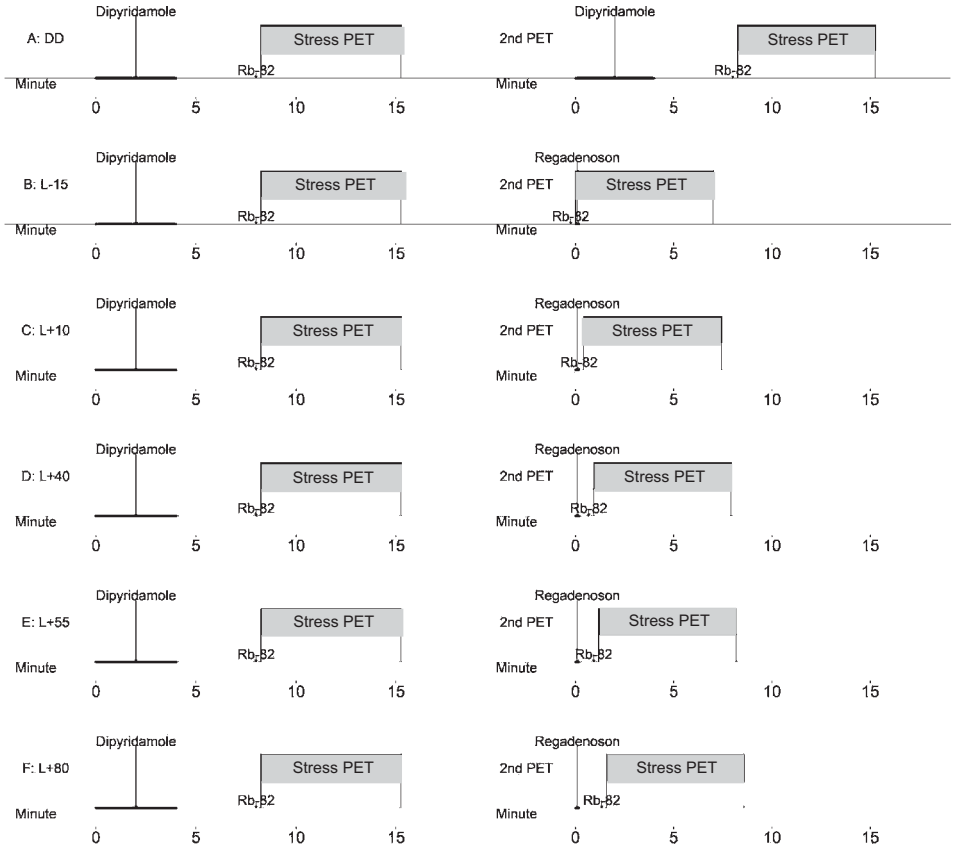

Fig. 4: Description of Protocols

Notes: The bold black line in the timeline denotes the duration of medication infusion, either dipyridamole or regadenoson. Protocols on the left is the scan using dipyridamole, while protocols on the right administered regadenoson with variable delays before injection of the Rb-82 radiotracer.

Tab. 1: Protocols

Protocol	Description
DD	Repeated dipyridamole
L - 15	Regadenoson group with Rb-82 activated 15 seconds prior to injection of regadenoson
L + 10	Regadenoson group with Rb-82 activated 10 seconds after injection of regadenoson
L + 40	Regadenoson group with Rb-82 activated 40 seconds after injection of regadenoson
L + 55	Regadenoson group with Rb-82 activated 55 seconds after injection of regadenoson
L + 80	Regadenoson group with Rb-82 activated 80 seconds after injection of regadenoson

2.2. STATISTICAL ANALYSIS

Statistical analysis was conducted with R version 3.5.1 (The R Foundation for Statistical Computing Platform: x86_64-w64-mingw32/x64 (64-bit)). Descriptive tables present means, standard deviations, percentages, and p-values. Categorical variables were compared used multiple chi-squared tests, or Fisher's exact test for variables with counts less than 5. Continuous variables were compared used t-tests. For each protocol, frequency plots present the averaged pixel distribution of CFC, plus cumulative frequency plots for the averaged pixel distribution of CFC. To analyze the PET data, the primary approach was to evaluate differences in the pixel distribution of CFC for the two scans via a spatially-adjusted KS test. To compare against traditional approaches, we conducted paired t-tests, original KS tests, KS tests with ICC adjustment, and spatially-adjusted KS tests, including associated p-values.

3. RESULTS

There were 188 subjects recruited and 176 of them finished the protocol. Excluded subjects had severe side effects (7), lack of intravenous access (2), or other reasons (2). Table 2 shows the number of subjects in each protocol, including demographic, clinical, and relative PET uptake results (Johnson and Gould, 2015). Subjects were balanced for most baseline characteristics, including risk factors, medications, and medical history, but not for age, body mass index, and some cholesterol fractions. PET uptake was consistent among protocols.

Tab. 2: Descriptive Table

	Population	Protocols						P-value
		DD	L-15	L + 10	L + 40	L + 55	L + 80	
Clinical characteristics								
Age	60 ± 9	62 ± 10	64 ± 8	57 ± 10	61 ± 7	60 ± 10	58 ± 6	0.02
BMI	29 ± 5	28 ± 5	27 ± 5	28 ± 4	30 ± 4	28 ± 5	31 ± 6	< 0.001
Risk factors and history								
Smoking	52(0.3)	16(0.32)	3(0.2)	17(0.34)	5(0.33)	9(0.29)	2(0.13)	0.66
MI	15(0.09)	4(0.08)	3(0.2)	4(0.08)	1(0.07)	2(0.06)	1(0.07)	0.72
Hypertension	81(0.46)	23(0.46)	10(0.67)	21(0.42)	7(0.47)	14(0.45)	6(0.4)	0.68
Dyslipidemia	132(0.75)	40(0.8)	10(0.67)	34(0.68)	14(0.93)	24(0.77)	10(0.67)	0.32
Diabetes	17(0.1)	7(0.14)	3(0.2)	4(0.08)	1(0.07)	2(0.06)	0(0)	0.39
Catheterization	38(0.22)	12(0.24)	4(0.27)	10(0.2)	5(0.33)	4(0.13)	3(0.2)	0.68
PCI	28(0.16)	8(0.16)	5(0.33)	8(0.16)	3(0.2)	1(0.03)	3(0.2)	0.19
CABG	8(0.05)	3(0.06)	2(0.13)	2(0.04)	0(0)	1(0.03)	0(0)	0.48
Medications								
Statin	89(0.51)	25(0.5)	10(0.67)	23(0.46)	11(0.73)	15(0.48)	5(0.33)	0.23
ACEI/ARB	48(0.27)	14(0.28)	3(0.2)	12(0.24)	7(0.47)	9(0.29)	3(0.2)	0.55
Antiplatelet	85(0.48)	17(0.34)	9(0.6)	27(0.54)	9(0.6)	17(0.55)	6(0.4)	0.20
Beta Blocker	50(0.28)	15(0.3)	8(0.53)	11(0.22)	5(0.33)	7(0.23)	4(0.27)	0.27
Diuretic	25(0.14)	7(0.14)	3(0.2)	7(0.14)	3(0.2)	4(0.13)	1(0.07)	0.91
Calcium blockers	14(0.08)	3(0.06)	1(0.07)	4(0.08)	2(0.13)	4(0.13)	0(0)	0.67
Nitrate	3(0.02)	1(0.02)	0(0)	1(0.02)	1(0.07)	0(0)	0(0)	0.65
Baseline Cardiac								

Cholesterol	180 ± 46	183 ± 50	153 ± 42	179 ± 38	155 ± 44	193 ± 43	216 ± 45	0.01
LDL	100 ± 36	102 ± 36	84 ± 30	98 ± 35	85 ± 39	105 ± 31	136 ± 32	0.01
HDL	54 ± 16	51 ± 16	54 ± 16	54 ± 14	50 ± 15	62 ± 19	51 ± 16	0.21
Rest Systolic blood pressure	115 ± 17	119 ± 19	117 ± 16	113 ± 16	114 ± 15	115 ± 16	112 ± 12	0.59
Rest Diastolic blood pressure	65 ± 10	68 ± 10	63 ± 10	63 ± 9	67 ± 14	64 ± 12	68 ± 6	0.26
Rest Heart Rate	63 ± 11	61 ± 10	60 ± 10	63 ± 11	64 ± 13	65 ± 12	66 ± 14	0.37
Stress Systolic blood pressure	119 ± 15	122 ± 17	111 ± 15	117 ± 15	121 ± 13	120 ± 15	120 ± 14	0.21
Stress Diastolic blood pressure	63 ± 10	64 ± 9	57 ± 12	61 ± 9	65 ± 14	64 ± 11	63 ± 8	0.19
Stress Heart Rate	89 ± 13	87 ± 13	83 ± 13	90 ± 13	92 ± 13	91 ± 13	93 ± 15	0.17
Non-baseline Cardiac								
Cholesterol	180 ± 46	185 ± 50	158 ± 43	178 ± 39	155 ± 44	193 ± 42	205 ± 46	0.03
LDL	100 ± 36	103 ± 36	87 ± 30	97 ± 36	85 ± 39	107 ± 31	127 ± 36	0.04
HDL	54 ± 17	51 ± 16	56 ± 16	55 ± 16	50 ± 15	61 ± 19	50 ± 15	0.29
Rest Systolic blood pressure	117 ± 16	117 ± 15	116 ± 18	116 ± 17	116 ± 24	117 ± 13	117 ± 14	0.99
Rest Diastolic blood pressure	67 ± 11	67 ± 9	63 ± 9	66 ± 12	68 ± 14	67 ± 9	70 ± 10	0.61
Rest Heart Rate	63 ± 12	60 ± 10	59 ± 8	65 ± 13	61 ± 9	67 ± 12	68 ± 15	0.03
Stress Systolic blood pressure	119 ± 19	120 ± 14	111 ± 18	119 ± 22	114 ± 21	124 ± 19	122 ± 18	0.29
Stress Diastolic blood pressure	62 ± 12	64 ± 10	61 ± 14	60 ± 14	62 ± 14	62 ± 11	63 ± 9	0.68
Stress Heart Rate	91 ± 15	85 ± 15	82 ± 12	96 ± 15	88 ± 11	98 ± 14	93 ± 13	< 0.001

Continuous variables presented as mean standard deviation; categorical variables presented as count(percentage)

BMI in kg per m^2

Systolic and diastolic Blood pressure in mmHg

Heart rate in beats per minute

Table 3 lists average rest perfusion, stress perfusion, and CFR. While resting perfusion did not differ significantly, stress perfusion and CFR changed among protocols, being higher with dipyridamole and variable among regadenoson timing sequences. A weak but noticeable positive correlation existed with timing such that later tracer injections tended to have higher CFR.

Tab. 3: Average rest perfusion, stress perfusion, and CFR among protocol

Protocol	Rest Perfusion			Stress Perfusion			CFR		
	Non-Base	Base	Δ	Non-Base	Base	Δ	Non-Base	Base	Δ
DD	0.79 ± 0.28	0.81 ± 0.27	-0.02 ± 0.2	2.13 ± 0.7	2.22 ± 0.65	-0.09 ± 0.46	2.78 ± 0.73	2.86 ± 0.76	-0.09 ± 0.7
L-15	0.73 ± 0.22	0.76 ± 0.23	-0.02 ± 0.18	1.3 ± 0.46	1.87 ± 0.61	-0.57 ± 0.4	1.78 ± 0.48	2.52 ± 0.73	-0.74 ± 0.75
L + 10	0.79 ± 0.28	0.78 ± 0.25	0.01 ± 0.24	1.71 ± 0.52	2.15 ± 0.61	-0.44 ± 0.48	2.25 ± 0.55	2.88 ± 0.79	-0.63 ± 0.72
L + 40	0.77 ± 0.24	0.76 ± 0.23	0.01 ± 0.22	1.79 ± 0.52	2.1 ± 0.55	-0.31 ± 0.38	2.43 ± 0.65	2.87 ± 0.69	-0.43 ± 0.79
L + 55	1.01 ± 0.37	0.96 ± 0.34	0.05 ± 0.21	2.28 ± 0.68	2.49 ± 0.71	-0.21 ± 0.42	2.36 ± 0.61	2.73 ± 0.78	-0.36 ± 0.77
L + 80	0.89 ± 0.32	0.87 ± 0.35	0.02 ± 0.23	2.14 ± 0.56	2.43 ± 0.74	-0.28 ± 0.49	2.53 ± 0.66	2.91 ± 0.65	-0.39 ± 0.56

Δ: The difference between base (first scan, dipyridamole) and Non-Base (second scan, variable stress medication).

Table 4 reports p-values from paired t-tests and KS tests with spatial adjustment, with similar trends to table 3. Spatial-adjusted KS produced smaller p-values than the paired t-test.

Tab. 4: P-values from paired t-test and spatially-adjusted KS test

Protocol	Rest Perfusion		Stress Perfusion		CFR	
	Paired t-test	Spatial KS	Paired t-test	Spatial KS	Paired t-test	Spatial KS
DD	0.483	0.288	0.094	0.004	0.221	$< 10^{-7}$
L-15	0.589	0.285	< 0.001	$< 10^{-16}$	< 0.001	$< 10^{-16}$
L+10	0.691	0.635	$< 10^{-10}$	$< 10^{-16}$	$< 10^{-10}$	$< 10^{-16}$
L+40	0.879	0.361	< 0.001	$< 10^{-16}$	0.013	$< 10^{-16}$
L+55	0.105	0.002	0.001	$< 10^{-9}$	0.004	$< 10^{-16}$
L+80	0.676	0.384	0.019	$< 10^{-13}$	< 0.001	$< 10^{-16}$

Figure 5 shows the average CFC distribution for each protocol. From the sub-plot 5(a), we found that the average CFC distribution for subjects in DD protocol (two dipyridamole scans) was almost comparable. Differences between baseline (dipyridamole) and non-baseline (regadenoson with variable timing) were due to medication/timing difference. The greatest differences between dipyridamole and regadenoson was observed in the L-15 protocol in sub-plot 5(b). Frequency plot showed that subjects administered with regadenoson and Rb-82 activated 15s prior to the drug administration in the baseline had a much higher frequency of mild/minimal reduced flow but a much lower frequency of good CFC compared to subjects administered with dipyridamole.

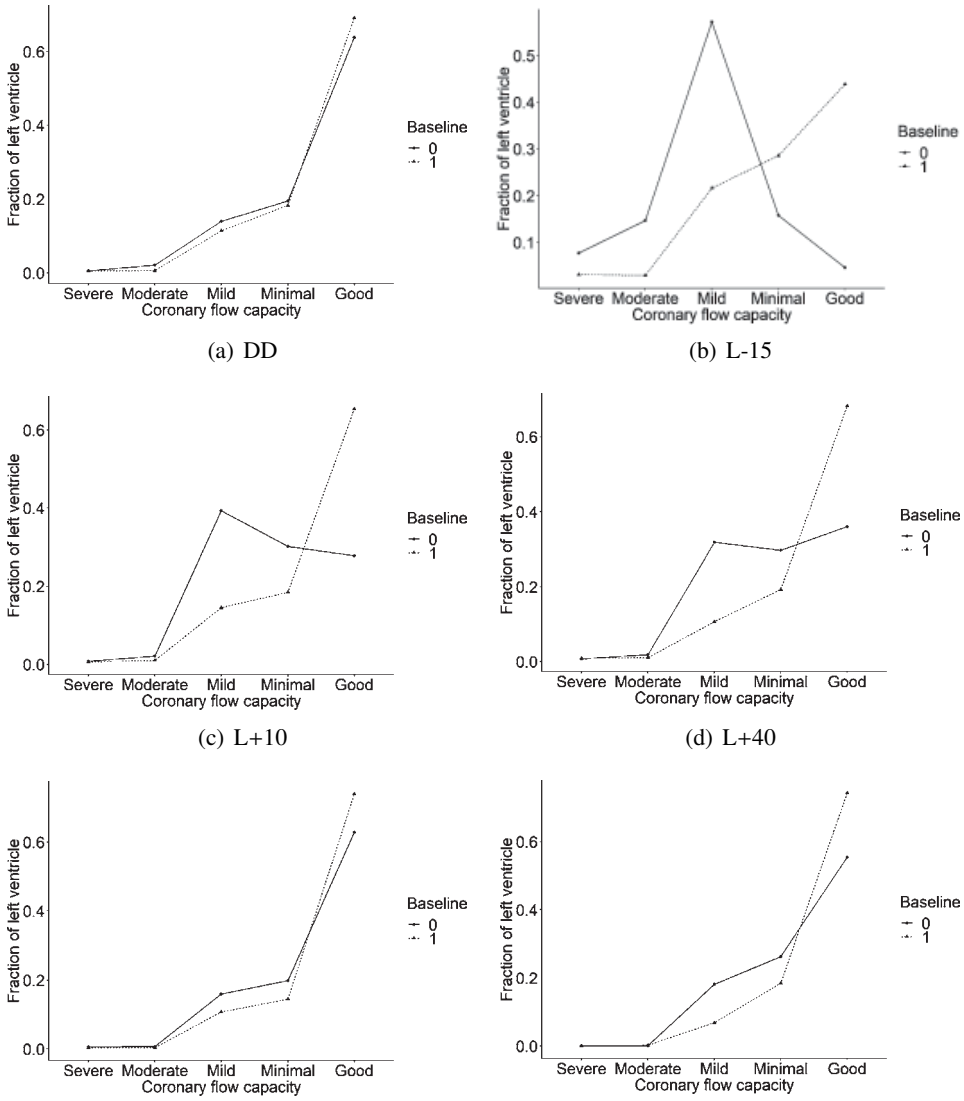

(a) DD (b) L-15

(c) L+10 (d) L+40

(e) L+55 (f) L+80

Fig. 5: CFC frequency plots of protocols

Similar trends were also presented in L+10 protocol and L+40 protocol. Protocols with a suitable delay, 55s, to activate Rb-82 after regadenoson was administered had the average pixel distribution of CFC comparable to its dipyridamole

baseline. A relatively lower frequency of pixels with good CFC was found in subjects with Rb-82 activated 80s after regadenoson bolus compared to their CFC using dipyridamole.

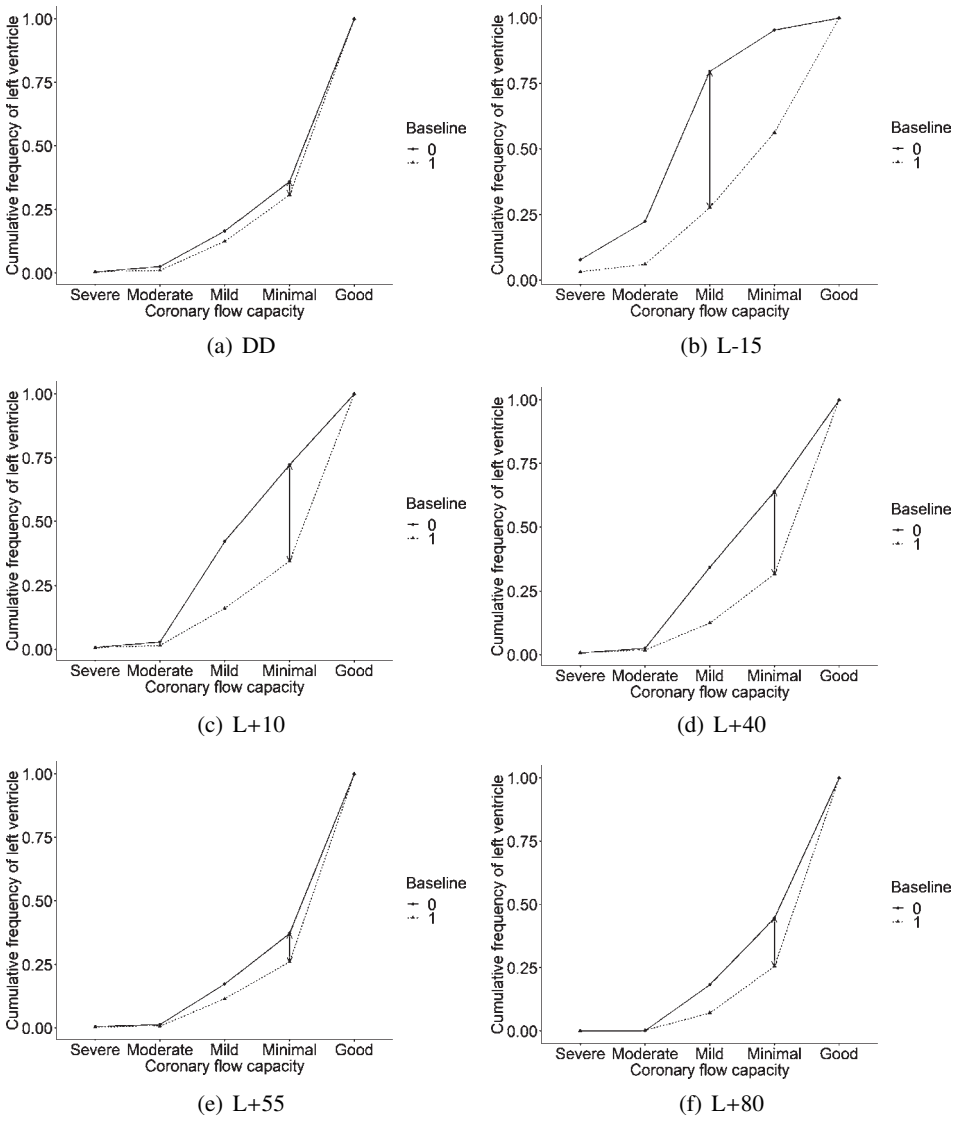

(a) DD (b) L-15

(c) L+10 (d) L+40

(e) L+55 (f) L+80

Fig. 6: Cumulative average CFC pixel frequency

Tab. 5: Kolmogorov-Smirnov Tests for Averaged Pixel Distribution of CFC

Protocol	KS statistic	P-Values		
		Spatial Adjusted KS	Original KS	ICC adjusted KS
DD	0.05	0.96	0.047	0.29
L - 15	0.52	$< 10^{-16}$	$< 10^{-16}$	$< 10^{-16}$
L + 10	0.38	$< 10^{-10}$	$< 10^{-16}$	$< 10^{-16}$
L + 40	0.32	$< 10^{-7}$	$< 10^{-16}$	$< 10^{-16}$
L + 55	0.11	0.24	$< 10^{-16}$	0.0004
L + 80	0.19	0.004	$< 10^{-16}$	$< e-10$

From the results in Figure 6 and Table 5 we found that the original KS test without any adjustment tends to give smaller p-values. Liberal p-values lead to an overestimation of the significance of the test result. Hence, using the original KS test without any adjustment, we may incorrectly conclude that all protocols, including the repeated dipyridamole group, reported a statistically significant difference in CFC distribution between baseline dipyridamole and the second scan, using either regadenoson or repeated dipyridamole.

With adjustment for the informative sample size, both the ICC-adjusted and spatially-adjusted KS tests reported higher p-values. It is worth noticing that the p-value from ICC-adjusted KS was relatively lower than that the spatially-adjusted KS. Average pixel distribution of CFC for subjects in L+55 protocol showed no statistically significant difference, based on the p-value reported from a spatially-adjusted KS test.

The KS tests for the L+80 protocol showed significant differences ($p = 0.004$) for the average pixel distribution of CFC. Results from CFC could be supported with the absolute differences in stress perfusion and CFR from table 4. Compared with baseline dipyridamole, the ordered protocols of absolute difference of stress perfusion are L - 15 > L + 10 > L + 40 > L + 80 > L + 55 > DD.

4. DISCUSSION AND CONCLUDING REMARKS

When positive spatial autocorrelation exists, the original KS overestimated significance and produced a p-value that was too small. ICC adjustment of the KS test reduces the p-values in the correct direction. However, ICC adjustment is not as effective as a KS test with spatial adjustment. Spatial-adjusted KS accounts for the effect of autocorrelation in spatial settings and therefore produced a p-value closer

to the true significance. Regardless of the scale of the existing correlation, the original KS test did not adjust the sample size. The ICC-adjusted KS test shrunk the sample size linearly while the spatially-adjusted KS test adjusted the sample size exponentially. The supremum of the absolute divergence of EDF between the dataset of interest and the second dataset using traditional KS, ICC-adjusted KS spatially-adjusted KS were the same. The differences in p-values from original, ICC-adjusted, and spatially-adjusted KS were due to variable adjustments of the informative sample size.

Our results partially agree with results from mixed-effects ANOVA of stress flow (Johnson and Gould, 2015). ANOVA results failed to detect the differences in the protocol of Rb-82 activated 80s after regadenoson bolus time. Analysis of average pixel distribution of CFC proved to be more accurate than only considering CFR or absolute perfusion. Our spatially-adjusted KS analysis of CFC provided an evaluation of the effectiveness of dipyridamole and different regadenoson timing protocols. Even though the difference of average CFC pixel distribution between dipyridamole and L+80 regadenoson was statistically significant, the clinical implications such differences requires further study. Based on our findings, physicians may evaluate the tradeoffs among timing protocols. A curvilinear hyperemic effect produced by different timings of the regadenoson bolus can be concluded from our reported results.

Our approach of analyzing PET scans may assist in future studies as it is simple to apply and easy to understand. In our trial, CFC is defined as a discontinuous variable determined by the CFR and stress perfusion. The KS test is a powerful tool for analyzing pixel distribution. However, it may lack power and be conservative when the underlying distribution is discrete (Conover, 1972; Gleser, 1985). A two-sample, spatially-adjusted KS test for discontinuous distribution is desired. Meanwhile, multi-dimensional KS tests have been studied by researchers (Justel et al., 1997). Multi-dimensional KS testing has proven to be a sensitive and powerful tool for discriminating images.(Metchev and Grindlay, 2002) Therefore, in future studies, we may consider proposing a multi-dimensional KS test with adjustment for spatial autocorrelation, permitting direct analysis of CFR and stress perfusion simultaneously.

The spatial autocorrelation coefficient is one of the fundamental pillars of the spatially-adjusted KS test. However, currently, there are no certain 'absolute' coefficients that account for spatial autocorrelation. By saying 'absolute' we mean that the spatial correlation coefficient was defined without any human-defining structure. Currently available coefficients were subjective in the sense that one

has to define the spatial structure and the correlation scale in regards to the spatial relationship between locations. For example, in this article, we assumed that the correlation between locations decays in proportion to the square of the distance. Another popular spatial correlation is the neighboring correlation weight function w_{ij} equal to 1 if X_i and X_j is adjacent and equal to 0 otherwise. A method that could evaluate the spatial correlation absolutely, without any subjective definition is needed and could be the topic for future studies.

Finally, we found that the regadenoson protocol with Rb-82 activated 55s after the injection of regadenoson has similar performance to dipyridamole from the results of the spatially-adjusted KS test. The protocols that inject radiotracer with other timing delays were sub-optimal compared to dipyridamole hyperemia.

Acknowledgement

This work was partially supported by Weatherhead Foundation.

REFERENCES

Adhyapak, S.M., Menon, P.G. and Rao Parachuri, V. (2013). Restoration of optimal ellipsoid left ventricular geometry: lessons learnt from in silico surgical modelling. In *Interactive CardioVascular and Thoracic Surgery,* 18 (2): 153–158.

Adhyapak, S. and Parachuri, V. (2010). Architecture of the left ventricle: insights for optimal surgical ventricular restoration. In *Heart Failure Reviews,* 15: 73–83.

Aston, J.A.D., Gunn, R.N., Worsley, K.J., Ma, Y., Evans, A.C. and Dagher, A. (2000). A statistical method for the analysis of positron emission tomography neuroreceptor ligand data. In *NeuroImage,* 12 (3): 245–256.

Azhari, H., Beyar, R. and Sideman, S. (1999). On the human left ventricular shape. In *Computers and Biomedical Research, an International Journal,* 32 (3): 264–282.

Baselice, F. (2017). Ultrasound image despeckling based on statistical similarity. In *Ultrasound in Medicine and Biology,* 43 (9):2065–2078.

Bozkurt, S. (2019). Mathematical modeling of cardiac function to evaluate clinical cases in adults and children. In *PLOS ONE,* 14 (10): 1–20.

Brook, O.R., Gourtsoyianni, S., Brook, A., Mahadevan, A., Wilcox, C. and Raptopoulos, V. (2012). Spectral ct with metal artifacts reduction software for improvement of tumor visibility in the vicinity of gold fiducial markers. In *Radiology,* 263 (3): 696–705. doi:10.1148/radiol.12111170.

Chen, J.W., Sans, M.Q., Bogdanov, J.A. and Weissleder, R. (2006). Imaging of myeloperoxidase in mice by using novel amplifiable paramagnetic substrates1. In *Radiology,* 240 (2): 473.

Conover, W.J. (1972). A kolmogorov goodness-of-fit test for discontinuous distributions. In *Journal of the American Statistical Association,* 67 (339): 591–596.

Cressie, N. (1992). Statistics for spatial data. In *Terra Nova,* 4 (5): 613–617.

DeKemp, R.A., Ruddy, T.D., Hewitt, T., Dalipaj, M.M. and Beanlands, R.S.B. (2000). Detection of serial changes in absolute myocardial perfusion with 82rb pet. In *Journal of Nuclear Medicine,* 41 (8): 1426–1435.

Geman, D., Geman, S., Gragne, C. and Dong, P. (1990). Boundary detection by constrained optimization. In *IEEE Transactions on Pattern Analysis and Machine Intelligence*, 12 (7): 609–628.

Gleser, L.J. (1985). Exact power of goodness-of-fit tests of Kolmogorov type for discontinuous distributions. In *Journal of the American Statistical Association*, 80 (392): 954–958.

Gould, K.L. and Johnson, N.P. (2018). Coronary physiology beyond coronary flow reserve in microvascular angina. In *Journal of the American College of Cardiology*, 72 (21): 2642–2662.

Hansen, F.K., Marinucci, D., Natoli, P. and Vittorio, N. (2002). Testing for non-gaussianity of the cosmic microwave background in harmonic space: An empirical process approach. In *Physical Review D - Particles, Fields, Gravitation and Cosmology*, 66 (6).

Herman, E. and Strang, G. (2016). *Calculus*. No. v. 3 in Open Textbook Library. OpenStax, Rice University.

Johnson, N.P. and Gould, K.L. (2015). Regadenoson versus dipyridamole hyperemia for cardiac pet imaging. In *JACC: Cardiovascular Imaging*, 8 (4): 438– 447.

Justel, A., Peña, D. and Zamar, R. (1997). A multivariate Kolmogorov-Smirnov test of goodness of fit. In *Statistics & Probability Letters*, 35 (3): 251–259.

Kershah, S., Partovi, S., Traughber, B.J., Jr., R.F.M., Schluchter, M.D., O'Donnell, J.K. and Faulhaber, P. (2013). Comparison of standardized uptake values in normal structures between pet/ct and pet/mri in an oncology patient population. In *Molecular Imaging and Biology*, 15 (6): 776–785.

Kipritidis, J., Hofman, M.S., Siva, S., Callahan, J., Roux, P.Y.L., Woodru, H.C., Counter,W.B. and Keall, P.J. (2016). Estimating lung ventilation directly from 4d ct hounsfield unit values. In *Medical Physics*, 43 (1): 33–43.

Kolmogorov, A. (1933). Sulla determinazione empirica di una legge di distribuzione. In *Inst.Ital.Attuari, Giorn.*, 4: 83–91.

Lampariello, F. (2000). On the use of the Kolmogorov-Smirnov statistical test for immunofluorescence histogram comparison. In *Cytometry*, 39 (3): 179–188.

Lim, D.H. and Jang, S.J. (2002). Comparison of two-sample tests for edge detection in noisy images. In *Journal of the Royal Statistical Society. Series D (The Statistician)*, 51 (1): 21–30.

Metchev, S.A. and Grindlay, J.E. (2002). A two-dimensional Kolmogorov-Smirnov test for crowded field source detection: Rosat sources in ngc 6397. In *Monthly Notices of the Royal Astronomical Society*, 335 (1): 73–83.

Mitchell, G.F., Lamas, G.A., Vaughan, D.E. and Pfeer, M.A. (1992). Left ventricular remodeling in the year after first anterior myocardial infarction: A quantitative analysis of contractile segment lengths and ventricular shape. In *Journal of the American College of Cardiology*, 19 (6): 1136–1144.

Moran, P.A.P. (1950). Notes on continuous stochastic phenomena. In *Biometrika*, 37 (1/2): 17–23.

Pettitt, A.N. and Stephens, M.A. (1977). The Kolmogorov-Smirnov goodness-of-fit statistic with discrete and grouped data. In *Technometrics*, 19 (2): 205–210.

Rajan, J., Dekker, A.J.D. and Sijbers, J. (2014). A new non-local maximum likelihood estimation method for rician noise reduction in magnetic resonance images using the Kolmogorov-Smirnov test. In *Signal Processing*, 103: 16–23.

Shepard, D. (1968). A two-dimensional interpolation function for irregularlyspaced data. ACM '68, 517-524. Association for Computing Machinery, New York, NY, USA.

Smirnov, N.V. (1939). On the Estimation of the Discrepancy Between Empirical Curves of Distribution for Two Independent Samples. In *Bul. Math. de l'Univ. de Moscou,* 2: 3–14.

Student (1908). The probable error of a mean. In Biometrika, 6 (1): 1–25.

Udelson, J.E. (2017). Left ventricular shape: The forgotten stepchild of remodeling parameters. In *JACC: Heart Failure,* 5 (3): 179 – 181.

Weiss, M.S. (1978). Modification of the Kolmogorov-Smirnov statistic for use with correlated data. In *Journal of the American Statistical Association,* 73 (364): 872–875.

Woods, R.H. (1892). A few applications of a physical theorem to membranes in the human body in a state of tension. In *Transactions of the Royal Academy of Medicine in Ireland,* 10 (1): 417.

Zheng, W. and Lai, D. (2019). Comparing heart pet scans: An adjustment of Komogorov-Smirnov test under spatial autocorrelation. In *Manuscript submitted for publication.*

Zheng, W., Lai, D. and Gould, K.L. (2019). A simulation study of a class of nonparametric test statistics: A close look of edf based tests. In *Manuscript submitted for publication.*